Polyoxometalates in Solution: Molecular Dynamics Simulations on the α-$PW_{12}O_{40}^{3-}$ Keggin Anion in Aqueous Media

Xavier López,[†] Carlos Nieto-Draghi,[‡] Carles Bo,[†,§] Josep Bonet Avalos,[‡] and Josep M. Poblet*[,†]

Departament de Química Física i Inorgànica, Facultat de Química, Universitat Rovira i Virgili, Marcel. lí Domingo s/n, 43007 Tarragona, Spain, Departament d'Enginyeria Quimica, Escola Tècnica Superior d'Enginyeria Química, Universitat Rovira i Virgili, Avda. dels Països Catalans 26, 43007, Tarragona, Spain, and ICIQ−Institut of Chemical Research of Catalonia, Avda. dels Països Catalans s/n, 43007 Tarragona, Spain

Received: July 15, 2004; In Final Form: October 1, 2004

The Keggin anion, $PW_{12}O_{40}^{3-}$, is one of the most representative polyoxometalates (POMs). In recent years increasing theoretical work focused on this family of compounds has explained or even predicted some of their properties using quantum mechanics methods. In this report we applied for the first time molecular dynamics (MD) to the title compound to analyze its interactions with water. We used three atomic charge definitions (Mulliken, ChelpG, and formal charges) to carry out MD simulations. The results show that the terminal oxygens of the cluster are invariably most effectively solvated by water because of their prominent position within the framework. On the other hand, bridging oxygens, which are confined in more internal positions, concentrate a smaller portion of the whole solvation. We investigated the hydrogen bonds existing between water and the cluster, confirming that the terminal positions form more contacts with H_2O than any other site of the cluster. In the end, the lifetime of such contacts is longer with bridging oxygens, presumably due to their higher atomic charge.

Introduction

Polyoxometalates (POMs)−or polyoxoanions−are medium-to-large clusters made up of metal cations and oxo ligands. They have distinctive chemical properties that have been studied since the 19th century that continue to attract the attention of scientists from various fields.[1] These structurally versatile inorganic compounds are studied and applied in catalysis, materials science, electrochemistry, and medicine.[2−3] In general, we may view their structure as an array of pseudo-octahedrally coordinated metal centers, MO_6, with $M^{n+} = d^0$ early-transition metals.[4] These polyoctahedral aggregates typically feature corner- and edge-sharing MO_6 units. The spherical Keggin phosphotungstate, $PW_{12}O_{40}^{3-}$, consists of a metal−oxide core made up of four corner-sharing trimers, W_3O_{13}, that surround an internal PO_4^{3-} unit. Within each trimer WO_6 units share edges (see Figure 1). This arrangement features the following oxygen types: the four PO_4 oxygens, isolated from the exterior, and the external oxygens, 12 of each type, labeled O_t (terminal oxygens), O_{b1} (between two edge-sharing octahedra), and O_{b2} (between two corner-sharing octahedra). The external oxygens are exposed to other molecules.

Since the first calculations on POMs,[5−6] most theoretical works have focused on the structure, electronic properties (redox, magnetism), and basicity of the oxygen sites.[7−8] Also, the majority of these studies assumed that POM molecules are in vacuo. This is often a good approximation because some of their properties are well reproduced in this context. However, reactions involving POMs mainly occur in solution, so introducing the external effects is sometimes fundamental. Such effects can be taken into account using two main techniques: one is with a continuum solvent model and the other with explicit molecules through classical mechanics methods. To date, a few articles on POMs have been reported using the former[9] but, to the best of our knowledge, no molecular dynamics (MD) simulations have been applied yet to large polyanions in liquid media. Since the chemistry of POMs entirely occurs in liquid media, it is important to investigate the solvent−solute interactions.

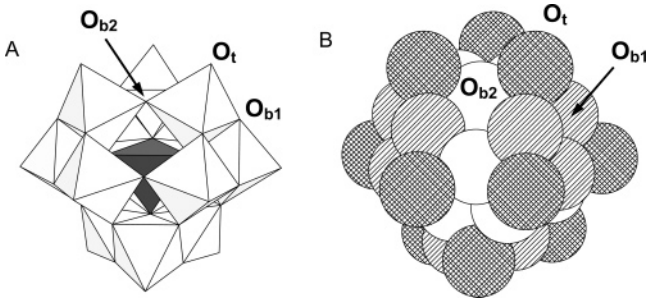

Figure 1. Keggin structure for α-$PW_{12}O_{40}^{3-}$. (A) Oxygen atom is located at each vertex of a WO_6 polyhedron, while the P atom is located in the center of the dark tetrahedron. (B) Space-filling representation with hatched spheres for terminal oxygens, stripped spheres for bridging oxygens of type 1 (O_{b1}), and empty spheres for type 2 bridging oxygens (O_{b2}). There are 12 oxygens of each type.

In this article the dynamics are analyzed classically because the de Broglie thermal length is much smaller than the distances between particles.[10] The dynamics are therefore fully governed by effective intermolecular potentials that are typically of the Lennard−Jones (LJ) type, with electrostatic interactions modeled through a given distribution of point charges. Since the Keggin

* To whom the correspondence should be addressed. E-mail: poblet@quimica.urv.es.
[†] Departament de Química Física i Inorgànica, Universitat Rovira i Virgili.
[‡] Departament d'Enginyeria Quimica, Universitat Rovira i Virgili.
[§] ICIQ−Institut of Chemical Research of Catalonia.

10.1021/jp046862u CCC: $30.25
Published on Web 01/25/2005

TABLE 1: Molecular Parameters for the SPC/E Model of Water

	ϵ (kJ mol^{-1})	σ (Å)	atomic charge
H	0.6502	3.17	+0.42
O_w			−0.85

TABLE 2: Molecular Parameters Used To Model the $PW_{12}O_{40}^{3-}$ Solute Anion[a]

				atomic Charge		
	d (Å)[b]	ϵ (kJ mol^{-1})	σ (Å)	Mulliken	CHelpG	formal
P	0.00	1.0264	3.00	+2.43	+1.51	+5
W	3.58	0.9250	2.34	+2.49	+3.81	+6
O_t	5.29	0.8975	3.17	−0.72	−0.85	−2
O_{b1}	3.97	0.8975	3.17	−0.93	−1.37	−2
O_{b2}	3.42	0.8975	3.17	−0.94	−1.55	−2

[a] Each atomic charge model was applied to a different MD run. [b] Distance to the center of the anion.

cluster is large, its dynamics depend more crucially on the long-range electrostatic forces than on the LJ dispersion forces.

We herein report the first MD study of a Keggin-containing aqueous solution. This type of modeling provides novel information on the solvent−solute interactions and can be important for understanding chemical reactions involving POMs. We characterize the solvation of the $PW_{12}O_{40}^{3-}$ anion (PW_{12} for short) in aqueous solution and the nature of the mutual H_2O−POM interactions. Three atomic charge models were applied to the MD study of the Keggin anion: two of them are commonly used in computational chemistry (Mulliken and CHelpG). The other simulation was carried out with formal charges to check the nature of the water−Keggin interactions due uniquely to structural reasons. We will discuss the three simulations in order to compare the performance of the atomic models.

Computational Details

We computed different structural and transport properties of aqueous solutions of the $Na_3[PW_{12}O_{40}]^{3-}$ Keggin anion through MD simulations. We used different atomic charge models to simulate the force field potentials of the POM: the Mulliken,[11] ChelpG,[12] and formal charges. To simulate water we used the SPC/E[13] model, and for Na^+ the model of Lee et al.[14] was introduced to make the system neutral. The simulation parameters for H_2O and $PW_{12}O_{40}^{3-}$ are listed in Tables 1 and 2, respectively. Due to the POMs structure the polyoxometalate−water potential is fully dominated by the electrostatic water−oxygen interactions. For oxygen we used fluoride LJ parameters extracted from the literature. [15] For phosphorus and tungsten the values were from the respective alkaline. In any case, the LJ parameters do not influence the results very much because the main effect comes from the electrostatic interactions and the partial charges, and this is precisely the effect this paper seeks to analyze.

The three right-hand columns of Table 2 contain the model charges. All the intermolecular interactions are represented by the two-body potential

$$U_{ij} = 4\epsilon_{ij}\left[\left(\frac{\sigma_{ij}}{r_{ij}}\right)^{12} - \left(\frac{\sigma_{ij}}{r_{ij}}\right)^{6}\right] + \frac{q_i q_j}{4\pi\epsilon_0 r_{ij}} \qquad (1)$$

where q_i is the atomic charge on site i, ϵ_{ij} and σ_{ij} are the LJ interaction parameters between sites i and j on different molecules, and $r_{ij} = |r_j - r_i|$ is the distance between the corresponding sites. Crossed interactions for the dispersive LJ forces were computed through the usual Lorentz−Berthelot rules, i.e., $\sigma_{ij} = 1/2(\sigma_i + \sigma_j)$ and $\epsilon_{ij} = (\epsilon_i\epsilon_j)^{1/2}$. We performed the simulations within the constant temperature ensemble, NVT, using a weak coupling bath[16] with a long-range correction for pressure and energy.[17] All simulations were carried out with 1000 molecules. The size of the cubic simulation box on the NVT ensemble was adjusted to fit a density of $\rho = 1.133$ g/cm^3. The equations of motion were integrated through a leapfrog[17] algorithm with a time step of 2 fs, while leapfrog implicit quaternions[18−19] were used to integrate the rotational part of the equations of motion. All the simulations were performed with periodic boundary conditions and the *reaction field* methodology[20] with the choice $\epsilon_{RF} \rightarrow \infty$ to account for the long-range electrostatic interactions. The reaction field and LJ cutoff lengths were set to 10 Å. A nearest-neighbor-list technique,[17] with a cutoff radius of 1.1 times the LJ radius, was also used. An equilibration run of 500 ps was done prior to each 2 ns production run to eliminate any memory of the initial conditions.

To analyze the dynamic behavior of the hydrogen bonds between POMs and water molecules, we used a geometrical criterion,[21] which was sufficient for our purpose. This criterion should fulfill three conditions:

(1) the distance R_{OO} between a given oxygen of the POM molecule and the oxygen atom of water must be less than R^c_{OO},

(2) the distance R_{OH} between the oxygen of the POM and the hydrogen corresponding to the water molecule must be less than R^c_{OH}, and

(3) the angle $\angle$H−O···O must be smaller than a given ϕ^c.

We used $R^c_{OH} = 2.5$ Å and $R^c_{OH} = 3.6$ Å, which correspond to the distance of the first minimum of the oxygen−oxygen radial distribution functions observed in pure water systems.[21,22] We used a value of 30° for ϕ^c. Because of the intermolecular vibrational motion inherent in the process of breaking and forming H bonds, the study of the dynamics of hydrogen bonds is not straightforward. We decided to compute the lifetime of the H bonds from the long-time decay of the autocorrelation functions[22,23]

$$C_{HB}(t) = \frac{\langle \eta_{ij}(t)\cdot\eta_{ij}(0)\rangle}{\eta_{ij}(0)^2} \approx \exp\left(\frac{-t}{t_{HB}}\right) (\text{as } t \rightarrow \infty) \qquad (2)$$

where the variable $\eta_{ij}(t)$ has a value of 0 or 1 depending on the H-bond state of a given pair of oxygen atoms. For instance, $\eta_{ij}(t) = 1$ if oxygens i and j are H bonded at time t, on condition that the bond has not been broken between 0 and t. Otherwise, $\eta_{ij}(t) = 0$. τ^c_{HB} is then obtained from an exponential fitting of the correlation function $C_{HB}(t)$ at long times, according to eq 2.[22,23b]

Prior to the MD simulations we obtained the optimized geometry for $PW_{12}O_{40}^{3-}$ with the ADF[24] program. The calculation was based on the local density approximation characterized by the $X\alpha$ model[25] with Becke's gradient-corrected functional[26] for exchange and the VWN parametrization[27] for correlation, corrected with Perdew's functional.[28] The basis set IV, which is triple-ζ + polarization Slater-type basis, was used as provided by the ADF library. The Mulliken charges were computed using ADF, whereas the CHelpG charges were obtained from a single-point Gaussian[29] run using the LANL2DZ basis set.[30]

The Mulliken model performs an arbitrary partition of space to comply with a given criterion of atomic size, thus assigning some electron density to each atom. In addition, this method strongly depends on the basis set used. The CHelpG model, on

TABLE 3: Diffusion Coefficients (*D*) and Coordination Numbers (N_c) Obtained in the Three Simulations

atomic charge model	D (cm^2/s)	N_c
Mulliken	3.2×10^{-6}	171
CHelpG	2.4×10^{-6}	180
formal	1.2×10^{-6}	206

the other hand, assigns atomic charges to reproduce the electrostatic field produced by the distribution of electrons and nuclei.

Results

We performed three MD simulations on the $Na_3PW_{12}O_{40} + H_2O$ system with the same set of parameters except for the atomic charges (see Table 2). As the electrostatic interactions between PW_{12} and H_2O are different in each case, so is the behavior of the water molecules in the vicinity of the POM. To emphasize these differences we analyzed (i) the diffusion coefficient, (ii) the radial distribution functions (RDF) of water molecules around several sites, and (iii) the hydrogen-bonding (HB) properties, i.e., the average number of HB formed upon Keggin$-H_2O$ contacts, $\langle N_{HB} \rangle$, and the HB lifetimes, τ_{HB}. Apart from the comparison of the models, the most important information obtained from the calculations is the structure and behavior of water in the vicinity of PW_{12}.

1. Calculation of Diffusion Coefficients. The diffusion coefficient, *D*, of the Keggin in solution can be computed from the mean square displacement of its center of mass in accordance with the well-known Einstein relation

$$D = \lim_{t \to \infty} \frac{\langle |r(t) - r(0)|^2 \rangle}{6t} \tag{3}$$

D is a measure of the mobility of a particle embedded in a solvent. Since the Keggin anion is large in comparison with the water molecule, the Stokes−Einstein equation

$$D \propto \frac{kT}{\eta r_h} \tag{4}$$

infers the hydrodynamic radius of the POM given the temperature *T* and the viscosity η of the solvent. Experimental values of diffusion coefficients for the Keggin anion were reported by Pope et al.[31] They measured $D = 3.36 \times 10^{-6}$ and 2.56×10^{-6} cm^2/s for acidic solutions of $PW_{12}O_{40}^{3-}$ and $SiW_{12}O_{40}^{4-}$, respectively. Grigoriev et al.[32] reported experimental *D* for several solutions of Keggin anions in a mixture of H_2O/alcohol. For $PVW_{11}O_{40}^{4-}$ they found values of *D* vs the concentration of countercation ranging from 2×10^{-6} to 3×10^{-6} cm^2/s. In our simulation on $PW_{12}O_{40}^{3-}$ (Table 3) we similarly obtained $D_{Mulliken} = 3.2 \times 10^{-6}$ cm^2/s and $D_{CHelpG} = 2.4 \times 10^{-6}$ cm^2/s. The error made in the evaluation of this magnitude is indeed extremely small (about 3 orders of magnitude smaller than *D*). As shown below, the differences in the simulated values of *D* obtained from the various charge models arise from the different amount of water molecules solvating PW_{12}. As the Stokes−Einstein equation states, the larger the *effective* hydrodynamic radius is, the smaller the diffusion. Plainly, we can say that if a solute molecule carries more waters of solvation, it moves more slowly. The Mulliken charges assigned to the oxo ligands are smaller than the CHelpG ones, so the surface negative charge that H_2O molecules feel is lower in the former case than in the latter case. This apparently leads to a poorer solvation of PW_{12} in the first model and, therefore, a smaller r_h, which thus produces a larger *D*. In fact, $D = 1.2 \times 10^{-6}$ cm^2/s with formal charges, which is much deviated from the experimental measurements and other simulations reported here. This is due to the exceedingly large charge assigned to the oxygen atoms. In our simulations we looked for a numerical relationship between *D* and the degree of solvation of PW_{12}. Typically, the effective hydrodynamic radius is a good estimate for the solvation of a solute. We also counted, for all simulations, the number of water molecules that filled a hypothetical sphere of radius ≤ 9 Å centered in the PW_{12} cluster. Table 3 compares, from the least to the most ionic model, the coordination numbers calculated. For Mulliken and CHelpG models the agreement between the theoretical and experimental values of *D* is good. As expected, formal charges perform poorly because this model fails to reproduce the electrostatic nature of the solute. The calculations also show that the more ionic the charge model, the higher the degree of solvation of PW_{12} and the smaller the value of *D*.

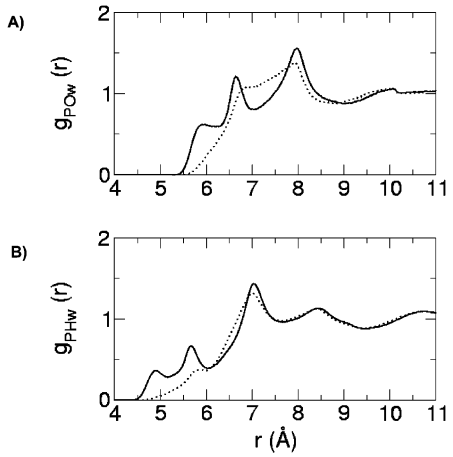

Figure 2. RDFs of water vs the distance from the center of the PW_{12} anion. The results from the Mulliken and CHelpG charge models are shown by dotted and solid lines, respectively. (A) RDF of O_w, and (B) RDF for H_w.

2. Radial Distributions and Hydrogen Bonding. *Mulliken Charges.* The dotted lines in Figure 2 show the result of simulating the aqueous solution on PW_{12} performed with the model of Mulliken charges. The solid lines show the results obtained from the model of CHelpG charges, which we will discuss later. Figure 2A represents the RDF for oxygens of waters as a function of the distance to the center of the Keggin anion, while Figure 2B represents the RDF for water hydrogens. The most remarkable feature of Figure 2A is the absence of well-defined peaks, which are replaced by a broad shoulder between 6.5 and 8 Å. The beginning of the shoulder is located between 6.5 and 7 Å. This distance corresponds to the location of the center of a water molecule in the vicinity of either oxygen O_{b1} or O_{b2}. The maximum of the shoulder is located close to 8 Å and corresponds to the position of water molecules that are forced to be around terminal oxygens (O_t) of the Keggin anion. However, the region between 5.5 Å and the beginning of the shoulder indicates some degree of penetration toward the vicinity of the most internal oxygen, which is referred to as O_{b2} (see Figure 1). The curve of Figure 2B is in agreement with that picture. The peak around 7 Å indicates some degree of localization of one hydrogen of a water molecule on the O_t oxygen, while the lower and broader peak around 8.5 Å corresponds to the other hydrogen of the same water molecule. The peak at 10.5 Å belongs to the second solvation shell. Finally, the small shoulder around 6 Å in Figure 2B corresponds to hydrogens attracted to O_{b1}.

More detailed information about the characteristics of the POM−water interaction is found in Figure 3. We show the

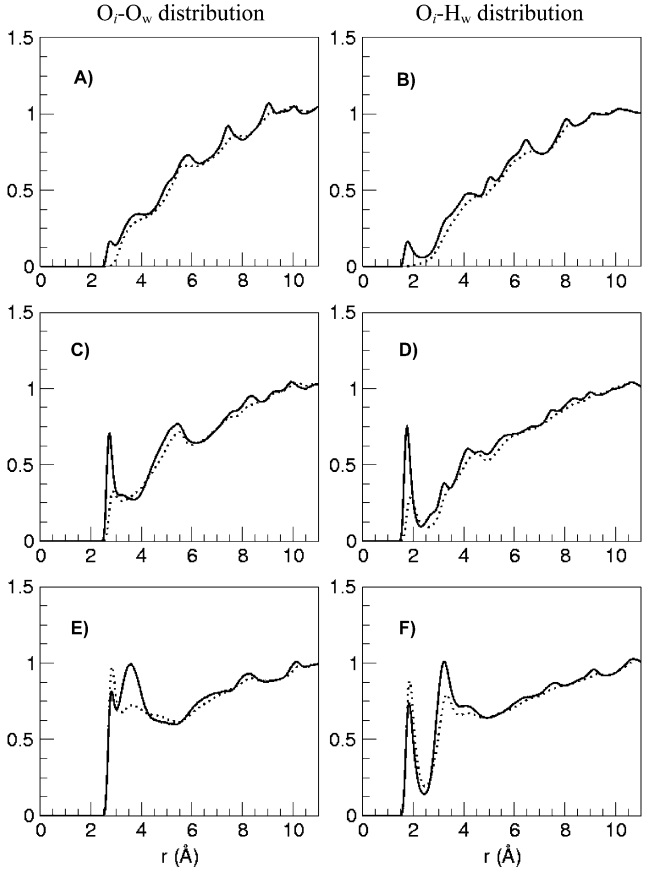

Figure 3. Three water-to-Keggin g(*r*) functions represented for the Mulliken (dotted lines) and the CHelpG (solid lines) charge models: (A and B) O_{b2}−water, (C and D) O_{b1}−water, and (E and F) O_t−water.

oxygen−oxygen and oxygen−hydrogen pair distribution functions between the three types of oxygens of the POM molecule and the corresponding oxygen (hydrogen) of the neighboring water molecules. In Figure 3A the position of water molecules refers to the O_{b2} sites of the Keggin anion. At distances closer than 10 Å the amount of water predicted by the Mulliken charges model (dotted line) progressively decreases and there are no noticeable peaks. This indicates that, within this model, the internal oxygen O_{b2} is not easily accessible. This interpretation is confirmed by Figure 3B. Figure 3C shows that a similar phenomenon takes place around site O_{b1}. However, the small peak around 2 Å in Figure 3D suggests some localization of waters around this bridge oxygen, O_{b1}. Figure 3E and F corresponds the POM's terminal oxygen, O_t. These oxygens are the sites that are most exposed to water contact since they are located at 5.29 Å from the center of the anion. There is an important localization of waters in the vicinity of the terminal oxygens. In Figure 3F the sharp peak of $g_{OtHw}(r)$ at 2 Å is indicative of the preferential orientation of water molecules around this position. The second peak corresponds to the second hydrogen of the same water molecule.

Figure 4A shows the correlation function $C_{HB}(t)$ for the three types of oxygens in PW_{12}. The curves clearly indicate the longer persistence of HB formed between terminal oxygens and H_w. We estimated the half-life time for the O_{b1} oxygen, $\tau_{Ob1} = 0.669$ ps, and for the O_t oxygen, $\tau_{term} = 1.142$ ps. Bearing in mind that there are 12 oxygen sites of each type (O_{b1}, O_{b2}, and O_t), the magnitude $\langle N_{HB} \rangle$ indicates how many water molecules are hydrogen bonded with the oxygens of each group. Figure 4C represents the probability distribution for N_{HB} for each species. The average number of HB for O_t is about three times larger than that of O_{b1}. In both cases the width of the distribution is about 5 HB. Since the charge of O_t is smaller than that of O_{b1} (see Table 2), O_t's the longer lifetime and greater number of HB compared to O_{b1} should be attributed to a more exposed position of O_t. For O_{b2}, the least exposed oxygen in PW_{12}, HB is hardly ever formed, so this oxygen contributes little to the solvation of the anion. On average, one-half of the O_{b1} sites are solvated while the other half are free of HB. The terminal oxygens are always solvated by at least one water molecule each ($\langle N_{HB} \rangle = 14.85$ over 12 O_t sites). These results for the model of Mulliken charges indicate that O_t sites are more efficiently solvated than O_{b1} sites. Essentially, this is due to the position of O_t rather than to its charge.

CHelpG Charges. A priori, a model based on CHelpG charges is more reliable than one based on Mulliken charges because CHelpG charges are fitted to reproduce the electrostatic potential at each point of space. Within this model the bridging oxygens of the Keggin anion become ∼50% more negatively charged

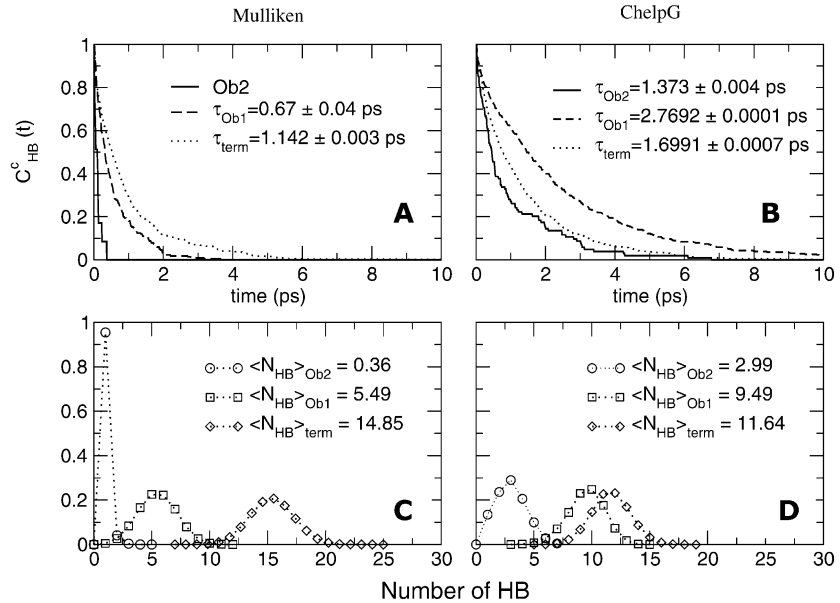

Figure 4. Lifetime of O_{b1}−H_w and O_t−H_w hydrogen bonds: (A) Mulliken and (B) CHelpG. Probability distribution of the number of hydrogen bonds (N_{HB}) on the 12 oxygens of each type in the POM. The legend shows the average number of each species: (C) Mulliken and (D) CHelpG.

than in the Mulliken model. In turn, the terminal oxygens are similarly charged in both models (see Table 2). Therefore, we expect a stronger attraction between PW_{12} and water molecules in the first solvation shell and a greater influence of bridging oxygens compared to terminal oxo sites. The first consequence of the greater attraction of the first solvation shell is that the diffusion coefficient of this model is smaller than that of the Mulliken model (Table 3).

The analysis of Figure 2 is similar to the analysis for the previous model. The most remarkable feature is the appearance of two well-defined peaks at 6.5 and 8 Å, where before we observed a broad band. With this model, therefore, the water molecules around O_{b1} and O_t are more localized. However, the larger charge of O_{b2} is responsible for the appearance of a shoulder between 5.5 and 6.5 Å that was absent in the previous case. Still, the hidden position of this oxo site prevents it from interacting strongly with water. Figure 2B agrees with this interpretation.

A thorough analysis with site-to-site $g(r)$ functions helps to explain the behavior of water around each oxo site. The solid and dashed lines in Figure 3 indicate the different structures of water depending on the model charges used. This difference is not evident in plots A and B, where $g_{Ob2-water}(r)$ only suffers from minor changes. These changes are summarized in a larger localization and a slightly larger population of water in the vicinity of the oxo site O_{b2}. There is a big increase in negative charge, however, for O_{b1} (Figure 3C and D). We can see a large peak in both of these figures, which indicates the presence of many water molecules at the surface of this oxygen site. O_{b1} now carries a similar charge to O_{b2} (-1.37), but the more exposed location of O_{b1}, 4 Å from the center of the cluster, allows H_w atoms to approach.

Note, however, the change in the shape of Figure 3E and F. Effectively, with respect to the Mulliken charge, the CHelpG charges predict a lower first peak around 2.5 Å and a much clearer peak at around 3.5 Å (Figure 3E). This may indicate a strong localization of water molecules in a region between the terminal oxygen and the O_{b1} oxo sites, which corresponds to enhancement of the first peak in Figure 3C. Parts F and E of Figure 3 have similar explanations and somehow indicate the presence of *bridging* water molecules, i.e., the two hydrogens are in the vicinity of O_t and O_{b1}, respectively. Note also the slightly more localized water hydrogens on O_{b1}, which are due to its greater atomic charge. Figure 3 may therefore indicate that increasing the charge in O_{b1} and O_{b2} oxo sites increases the contribution of these oxygens to the solvation of the Keggin anion and even slightly reduces the importance of the terminal oxygens as far as the water−Keggin interactions are concerned.

The half-lives of HB between water and the different oxo sites and the average number of HB formed to each site provide complementary information about the water−Keggin anion interaction (see Figure 4B and D). Figure 4B shows that the half-life of HB formed with O_{b1} is the largest and significantly larger than the lifetimes predicted with Mulliken charges. O_{b2} sites, formally free of waters in the Mulliken model, now form HB with a half-life of 1.4 ps. Figure 4D corresponds to the probability distribution of the number of HB assigned to each oxo site. Here, the average values relative to O_{b1} and O_t sites are similar: $\langle N_{HB}\rangle = 9.49$ and 11.64, respectively. Moreover, the average number of HB on O_t sites is lower than the predictions with Mulliken charges (Figure 4B), even though the net charge of the site is higher. This agrees with the interpretation of the set of pair distribution functions (Figure 3A−F) O_{b2} still tends less to capture H_2O molecules in its vicinity. Recall

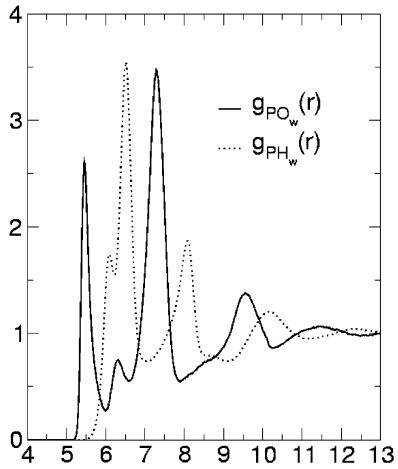

Figure 5. Joint representation of the RDF of O_w and H_w for the model simulation of formal charges. The horizontal scale refers to the center of the Keggin cluster. The vertical scaling is the same as that in the other figures.

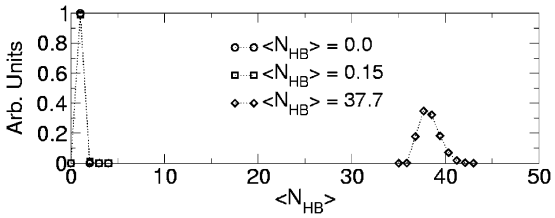

Figure 6. Mean number of hydrogen bonds for the formal charge model simulation. The only relevant signal corresponds to HB formed between H_w and O_t.

that while $\langle N_{HB}\rangle$ for O_{b1} is lower than for O_t, the time spent by each H_2O molecule in the vicinity of the former is the largest in this simulation. Therefore, the most accessible sites are terminal oxygens. However, HB are stronger between H_2O and O_{b1}, though these oxygens are less accessible. This indicates the competition between the position of the oxygen and its atomic charge.

Formal Charges. Formal atomic charges were applied to PW_{12} to allow the solvent to be affected only by the structure of the solute. This simulation is less rigorous than the previous ones, but it helps to separate the electrostatic effects from the structural effects in solvation phenomena. Since all the oxygen atoms of PW_{12} carry a negative charge of -2, the nature of their interactions with the solvent differs due to structural factors exclusively. Figure 5 shows the $g_{P-Ow}(r)$ and $g_{P-Hw}(r)$ functions. $g_{P-Hw}(r)$ is characterized by one high band at 6.5 Å, which is accompanied by a shoulder of lower intensity at 6.0 Å. These two peaks may be associated with solvation of the terminal oxygens, though the shoulder at 6.0 Å may be related to the approach of some water molecules to O_{b1}. Actually, this peak is far from O_{b1} (the P−O_{b1} distance is 3.97 Å). In previous charge models that displayed a peak of $g_{P-Hw}(r)$ associated with O_{b1} it appeared at ∼5.7 Å, which was 0.3 Å closer to P. The $g_{P-Ow}(r)$ radial function features a sharp high band at 5.5 Å. What are the H_w associated with this band? Comparing the two plots we think that g_{P-Ow} (5.5 Å) is associated with g_{P-Ow} (6.0 Å). This may indicate that the H_2O molecules whose O_w atoms are at 5.5 Å are oriented *outward* from the PW_{12} anion to enable the O_w atoms to be close to W^{6+}. The HB analysis can help us to assign these bands. Figure 6 shows the average number of hydrogen bonds formed between H_2O and each oxygen site of PW_{12}. The only site that features bonding to H_w is the terminal oxygen. We may say that, on average, all the terminal positions

form at least 2−3 HB with water molecules. The other oxygens are virtually free of waters.

To end our discussion of the results we will examine the acid−base properties of POMs. In some structures the controversial point of "which is the most basic site", as for the Keggin heteropolyanion discussed here, is still being investigated. Previous calculations to determine basicity scales of iso-[6,33] and heteropoly-[7d,9a,34] anions invariably proposed bridging oxygens as the most basic sites.[35] However, these studies accounted only for the *thermodynamic* relative stability of the species and did not consider the *dynamic* factor. On the other hand, IR[36] and REDOR NMR[7d] data suggested that protons in Keggin clusters could preferentially be attached at the terminal oxygens. Our MD simulations with Mulliken and CHelpG charges are in agreement with this possibility.

Many reports showed that the motion of H^+ in protic solvents is unusual. Today it is believed that the mechanism for proton transport in water involves H^+ hopping between H_2O units by formation−annihilation of covalent and hydrogen bonds.[37−38] Our present results show that the highest water concentration around the Keggin anion occurs at O_t sites and that these sites are the most effectively solvated. If the mechanism for proton transport really governs the acid−base reactions, our results could explain the protonation at terminal sites in Keggin anions. Water distributions suggest that the kinetics of the protonation reaction may balance the thermodynamic difference between protonation at a terminal site and a bridging site.[9a]

Summary and Conclusions

We performed a molecular dynamics study on an aqueous solution with composition $[Na_3PW_{12}O_{40}]$. Three models were used to characterize the Keggin anion: Mulliken, ChelpG, and formal atomic charges as well as the standard SPC/E model for water and the Na^+ cation. From these simulations, we traced common features between these models to describe the nature of water in the vicinity of a POM solute. We can conclude the following. (i) Provided that our solute molecule is anionic, the first solvation shell contains water molecules that are oriented so that their H atoms point toward the Keggin cluster. (ii) The region with the greatest accumulation of water is located at distances 6−9 Å from the center of the cluster. (iii) Two factors determine the extent of solvation on each site of the cluster: the atomic charge and the position. The most effectively solvated site by H_2O molecules is the terminal oxygen because, although it carries the lowest negative charge, it is the most external. On the other hand, the bridging oxygens O_{b2}, the most internal ones, are poorly solvated in all models. (iv) The degree of solvation of oxygens in the Keggin anion increases as their negative charge does.

The most reliable of the charge models applied in this study is probably the ChelpG. This model properly describes the ionic nature of POMs by reproducing the electrostatic potential generated by the distribution of nuclei and electrons. This is a feature that other models do not account for. Several properties, such as the RDF or the average number of HB, show that solvation mainly occurs at the terminal sites, O_t, and to a lower extent at the O_{b1} bridging oxygens. Both sites form a number of HB with water molecules close to one per site, on average. In both charge models the terminal oxygens are the least negatively charged but their external position in the framework allows them to be surrounded by more water molecules than the bridging oxygens. From the simulation with formal charges (ionic model) we showed that the structural factor forces the solvent molecules to remain attached to terminal oxygens. In fact, bridging oxygens are free of waters, which indicates the importance of the position in the cluster.

Two important features support the validity of our analyses. First, the diffusion coefficients are close to the experimental values, and second, the terminal oxygens for the PW_{12} anion are the most likely ones to be protonated (largest number of HB bonds), a prediction that is also in agreement with experimental data.

In future projects we will study $XM_xW_{12-x}O_{40}$ mixed-metal Keggin anions, Lindqvist structures, and larger POMs whose chemistry is very interesting, for example, in processes of polymerization and assembly. We also intend to include variables such as the ionic strength when modeling POMs in solution. Other studies[31,39] have shown that this and the nature of the counterions are crucial parameters for the structure and properties of some POMs.

Acknowledgment. This work was supported by the Spanish MCyT (BQU2002-04110-C02-01, PPQ2000-2888-E, PPQ 2001-0671), the CIRIT of the Generalitat de Catalunya (Autonomous Government of Catalonia) (SGR01-00315, ACI2000-13, ACI2001-39, and ACI2002-37), and the Rovira i Virgili University (2000PIR-21). We thank Dr. Allan Mackie for his helpful comments.

References and Notes

(1) In *Polyoxometalate Molecular Science*; Borrás-Almenar, J. J., Coronado, E., Müller, A., Pope, M. T., Eds.; NATO Science Series 98; Kluwer Academic Publishers: Dordrecht, 2003.

(2) Hill, C. L., Ed. *Chem. Rev.* **1998**, *98*, 359.

(3) In *Polyoxometalates: From Platonic Solids to Anti-Retroviral Activity*. Pope, M. T., Müller, A., Eds.; Kluwer Academic Publishers: Dordrecht, 1994.

(4) Pope, M. T. *Heteropoly and Isopoly Oxometalates;* Springer-Verlag: Berlin, 1983.

(5) Taketa, H.; Katsuki, S.; Eguchi, K.; Seiyama, T.; Yamazoe, N. *J. Phys. Chem.* **1986**, *90*, 2959.

(6) Kempf, J. Y.; Rohmer, M.-M.; Poblet, J.-M.; Bo, C.; Bénard, M. *J. Am. Chem. Soc.* **1992**, *114*, 1136.

(7) Rohmer, M.-M.; Bénard, M.; Blaudeau, J.-P.; Maestre, J. M.; Poblet, J. M. *Coord. Chem. Rev.* **1998**, *178−180*, 1019.

(8) (a) Maestre, J. M.; López, X.; Bo, C.; Daul, C.; Poblet, J. M. *Inorg. Chem.* **2002**, *41*, 1883. (b) Bridgeman, A.; Cavigliasso, G. *J. Phys. Chem. A* **2002**, *106*, 6114. (c) Bridgeman, A.; Cavigliasso, G. *Inorg. Chem.* **2002**, *41*, 1761. (d) Ganapathy, S.; Fournier, M.; Paul, J. F.; Delevoye, L.; Guelton, M.; Amoureux, J. P. *J. Am. Chem. Soc.* **2002**, *124*, 7821. (e) Poblet, J. M.; López, X.; Bo, C. *Chem. Soc Rev.* **2003**, *32*, 297.

(9) (a) López, X.; Bo, C.; Poblet, J. M. *J. Am. Chem. Soc.* **2002**, *124*, 12574. (b) López, X.; Fernández, J. A.; Romo, S.; Paul, J. F.; Kazansky, L.; Poblet, J. M. *J. Comput. Chem.* **2004**, *25*, 1542.

(10) Hansen J. P.; McDonald I. R. *Theory of simple liquids*, 2nd ed.; Academic Press: London.

(11) Mulliken, R. S. *J. Chem. Phys.* **1955**, *23*, 1833.

(12) Breneman, C. M.; Wiberg, K. B. *J. Comput. Chem.* **1990**, *11*, 361.

(13) Berendsen, H. J. C.; Grigera, J. R.; Straasma, T. P. *J. Phys. Chem.* **1987**, *91*, 6269.

(14) Lee, S.; Rasaiah, J. *J. Phys. Chem.* **1996**, *100*, 1420.

(15) Dang, L. X. *J. Chem. Phys.* **1992**, *96*, 6970.

(16) Berendsen, H. J. C.; Postma, J. P. M.; van Gunsteden, W. F.; DiNola, A.; Haak, J. R. *J. Phys. Chem.* **1984**, *81*, 3684.

(17) Allen, M. P.; Tildesley, D. J. *Computer Simulation of Liquids*, 1st ed; Clarendon Press: Oxford, 1989.

(18) Evans, D. J. *Mol. Phys.* **1997**, *34*, 317.

(19) Svanberg, M. *Mol. Phys.* **1997**, *92*, 1085.

(20) Neuman, M. *J. Chem. Phys.* **1986**, *85*, 1567.

(21) Martí, J. *J. Chem. Phys.* **1999**, *110*, 6876.

(22) Nieto-Draghi, C.; Bonet Avalos, J.; Rousseau, B. *J. Chem. Phys.* **2003**, *119*, 4782.

(23) (a) Guàrdia, E.; Martí, J.; Padró, J.; Komolkin, A. V. *J. Mol. Liq.* **2002**, *96*, 3. (b) Matsumoto, M.; Gubbins, K. E. *J. Chem. Phys.* **1990**, *93*, 1981.

(24) ADF 2003. Department of Theoretical Chemistry, Vrije Universiteit. Amsterdam. Baerends, E. J.; Ellis, D. E.; Ros, P. *Chem. Phys.* **1973**, *2*, 41. Versluis, L.; Ziegler, T. *J. Chem. Phys*. **1988**, *88*, 322. Te Velde, G.; Baerends, E. J. *J. Comput. Phys*. **1992**, *99*, 84. Fonseca Guerra, C.; Snijders, J. G.; Te Velde, G.; Baerends, E. J. *Theor. Chem. Acc*. **1998**, *99*, 391.

(25) Slater, J. C. *Quantum Theory of Molecules and Solids*; McGraw-Hill: New York, 1974; Vol. 4.

(26) Becke, A. D. *J. Chem. Phys*. **1986**, *84*, 4524. Becke, A. D. *Phys. Rev*. **1988**, *A38*, 3098.

(27) Vosko, S. H.; Wilk, L.; Nusair, M. *Can. J. Phys*. **1980**, *58*, 1200.

(28) Perdew, J. P. *Phys. Rev*. **1986**, *B33*, 8822. Perdew, J. P. *Phys. Rev*. **1986**, *B34*, 7406.

(29) Frisch, M. J.; Trucks, G. W.; Schlegel, H. B.; Scuseria, G. E.; Robb, M. A.; Cheeseman, J. R.; Zakrzewski, J. A.; Montgomery, J. A.; Stratman, R. E.; Burant, J. C.; Dapprich, S.; Millam, J. M.; Daniels, A. D.; Kudin, K. N.; Strain, M. C.; Farkas, O.; Tomasi, J.; Barone, V.; Cossi, M.; Cammi, R.; Mennucci, B.; Pomelli, C.; Adamo, C.; Clifford, S.; Ochterski, J.; Petersson, G. A.; Ayala, P. Y.; Cui, Q.; Morokuma, K.; Malick, D. K.; Rabuck, A. D.; Raghavachari, K.; Foresman, J. B.; Cioslowski, J.; Ortiz, J. V.; Stefanov, B. B.; Liu, G.; Liashenko, A.; Piskorz, P.; Komaromi, I.; Gomperts, R.; Martin, R. L.; Fox, D. J.; Keith, T.; Al-Laham, M. A.; Peng, C. Y.; Nanayakkara, A.; González, C.; Challacombe, M.; Gill, P. M. W.; Johnson, B. G.; Chen, W.; Wong, M. W.; Andres, J. L.; Head-Gordon, M.; Replogle, E. S.; Pople, J. A. *Gaussian 98*; Gaussian, Inc.: Pittsburgh, PA, 1998.

(30) Hay, P. J.; Wadt, W. R. *J. Chem. Phys*. **1985**, *82*, 299. Dunning, T. H., Jr.; Hay, P. J. In *Modern Theoretical Chemistry;* Schaefer, H. F., III, Ed.; Plenum: New York, 1976; pp 1−28.

(31) Pope, M. T.; Varga, G. M. *Inorg. Chem*. **1966**, *5*, 1249.

(32) Grigoriev, V. A.; Hill, C. L.; Weinstock, I. A. *J. Am. Chem. Soc*. **2000**, *122*, 3544. Grigoriev, V. A.; Cheng, D.; Hill, C. L.; Weinstock, I. A. *J. Am. Chem. Soc*. **2000**, *123*, 5292.

(33) Maestre, J. M.; Sarasa, J. P.; Bo, C.; Poblet, J. M. *Inorg. Chem*. **1998**, *37*, 3071.

(34) Bardin, B. B.; Bordawekar, S. V.; Neurock, M.; Davis, R. J. *J. Phys. Chem. B* **1998**, *102*, 10817.

(35) The protonation at a bridging site was computed to be ∼11 kcal mol^{-1} lower than at a terminal site in PW_{12}. Similarly, in PMo_{12} this difference was 19 kcal mol^{-1} (see refs 8d and 9a).

(36) Rocchicioli-Deltcheff, C.; Aoussi, A.; Bettahar, M. M.; Launay, S.; Fournier, M. *J. Catal.* **1996**, *164*, 16.

(37) Marx, D.; Tuckerman, M. E.; Hutter, J.; Parrinello, M. *Nature* **1999**, *397*, 601.

(38) Kornyshev, A. A.; Kuznetsov, A. M.; Spohr, E.; Ulstrup, J. *J. Phys. Chem. B* **2003**, *107*, 3351.

(39) Knoth, W. H.; Harlow, R. L. *J. Am. Chem. Soc*. **1981**, *103*, 1865. Contant, R.; Tézé, A. *Inorg. Chem*. **1985**, *24*, 4610. Canny, J.; Tézé, A.; Thouvenot, R.; Hervé, G. *Inorg. Chem.* **1986**, *25*, 2114. Jorris, T. L.; Kozok, M.; Baker, L. C. W. *Inorg. Chem.* **1990**, *29*, 4584. Kirby, J. F.; Baker, L. C. W. *Inorg. Chem.* **1998**, *37*, 5537.